Supplementary information: Elucidation of photovoltage origin and charge transport in Cu_2O heterojunctions for solar energy conversion

Peter Cendula,*[a,b], Matthew T. Mayer,[c,d], Jingshan Luo,[c,e] and Michael Grätzel,[c]

[a] *Institute of Aurel Stodola, Faculty of Electrical Engineering and Information Technology, University of Zilina, kpt. Nalepku 1390, 03101 Liptovsky Mikulas, Slovakia. Tel: +421-41-513-1484; E-mail: peter.cendula@fel.uniza.sk*
[b] *Institute of Computational Physics, Zurich University of Applied Sciences (ZHAW), Wildbachstrasse 21, 8401 Winterthur, Switzerland.*
[c] *Laboratory of Photonics and Interfaces, Ecole Polytechnique Fédérale de Lausanne, EPFL-SB-ISIC-LPI, Station 6, 1015 Lausanne, Switzerland.*
[d] *Helmholtz-Zentrum Berlin für Materialien und Energie, Hahn-Meitner-Platz 1, 14109 Berlin, Germany.*
[e] *Institute of Photoelectronic Thin Film Devices and Technology, College of Electronic Information and Optical Engineering, Nankai University, 38 Tongyan Road, Jinnan District, Tianjin, 300350 China.*

1 Theory

Drift-diffusion equations we used for description of charge transport in the photocathode

$$\frac{d^2\phi}{dx^2} = -\frac{q(N_D - n(x) + p(x) - N_A)}{\varepsilon_0\varepsilon_r}, \quad (1)$$

$$0 = +\frac{1}{q}\frac{\partial j_e}{\partial x} + G(x) - R(x), \quad (2)$$

$$0 = -\frac{1}{q}\frac{\partial j_h}{\partial x} + G(x) - R(x), \quad (3)$$

where $q = 1.6 \cdot 10^{-19}$ C is elementary electron charge, ϕ, n, p denote electrostatic potential, electron and hole concentration and x spatial coordinate. Donor(acceptor) concentration is denoted $N_D(N_A)$, permittivity of vacuum ε_0, relative dielectric constant ε_r, generation rate $G(x)$ and recombination rate $R(x)$.

The electron and hole flux j_e, j_h consists of two terms (diffusion and drift)

$$j_e = +qD_e\frac{\partial n}{\partial x} - q\mu_e n\frac{\partial \phi}{\partial x}, \quad (4)$$

$$j_h = -qD_h\frac{\partial p}{\partial x} - q\mu_h p\frac{\partial \phi}{\partial x}, \quad (5)$$

where the electrostatic potential is ϕ, electron mobility is μ_e and hole mobility μ_h.

Illumination source AM1.5G with intensity 100 mW/cm^2 was applied from the electrolyte side,[20] and for simplicity light absorption in TiO_2, AZO and Ga_2O_3 layers was neglected due to their wide bandgaps in comparison to that of Cu_2O. Optical reflections at all interfaces are also neglected. The generation rate of charge carriers from the simple Lambert-Beer law was assumed with wavelength-dependent absorption coefficient of Cu_2O.[15] Shockley-Read-Hall recombination through a midgap state is assumed in all layers and the corresponding carrier lifetimes are computed from the mobility and diffusion length values in Table S1.

The model equations were numerically solved in Comsol Multiphysics software.[1] The baseline material parameters are summarized in Table S1. We remark that our baseline parameters assume perfect CB alignment of Cu_2O and Ga_2O_3 (equal value of χ), although various small offsets (positive or negative) have been reported in the literature. We always refer applied voltage with respect to dark equilibrium (for HER taking place at photocathode, this translates to voltage versus the reversible hydrogen electrode, RHE). The total cathodic current density in photocurrent-voltage (IV) plots is reported negative as usual for photocathodes.[6] Different to this sign convention for total current in our IV plots, positive electron current density indicates flow of electrons from right (Cu_2O) to the left (electrolyte) in our figures, whereas positive hole current density is in the opposite direction. Thus, positive (negative) partial current density means flow of that carrier in the desired (undesired) direction for forward operation of HER on the photocathode. As a replacement of the quantity V_{oc} used in photovoltaics, we use the broadly used term of photocurrent onset (turn-on) voltage V_{on} for photoelectrodes,[4] defined as voltage for which photoelectrode starts to sustain measurable photocurrent (here we chose 0.1 mA/cm^2 threshold).

Stable numerical convergence of the model requires better mesh quality close to the internal interfaces. Therefore, the Cu_2O was meshed by 500 elements of symmetric arithmetic distribution, whereas TiO_2 and Ga_2O_3 were meshed with 500 elements (element ratio 10) with geometric distribution refined to the left of TiO_2 and Ga_2O_3, respectively. Where convergence was not obtained from the predefined initial values in Comsol, we used solution at thermal equilibrium as initial value for the solution away from thermal equilibrium.

Symbol	TiO_2	AZO	Ga_2O_3	IRL	Cu_2O	Description
d [nm]	50	50	50	10	260	Thickness
N_D [cm^{-3}]	$2 \cdot 10^{17}$	10^{20}	10^{16}[11]	0	0	Donor concentration
N_A [cm^{-3}]	0	0	0	$5 \cdot 10^{17}$[23]	$5 \cdot 10^{17}$[23]	Acceptor concentration
m_e [m_0]	10[8]	0.2[25, 9, 17]	0.3[10]	0.99 [12]	0.99 [12]	Effective mass of electron
m_h [m_0]	0.8[8]	0.8[25]	5[10]	0.58 [12]	0.58 [12]	Effective mass of hole
χ [eV]	4.4[3]	4.4[24]	3.2[3]	3.2[3]	3.2[3]	Electron affinity
ε_r	75	9[25]	9	6.6	6.6	Relative permittivity
E_g [eV]	3.2	3.35[25]	5	2.17	2.17	Bandgap energy
μ [$cm^2V^{-1}s^{-1}$]	20[18]	10	10^2[14, 13]	2.5[22, 19]	2.5[22, 19]	Electron and hole mobility
L [nm]	10 000 [16]	150[2]	300[13]	50 [22]	50 [22]	Carrier diffusion length

Table S1: Baseline material parameters of semiconductors used in the calculations. The donor traps with density $5 \cdot 10^{17}$ cm^{-3} in IRL are assumed to have 0.1 V wide Gaussian distribution around midgap with capture electron (hole) capture cross-section of $5 \cdot 10^{-13}$ cm^2 (10^{-15} cm^2), respectively.

2 Estimations of built-in voltage

We will calculate built-in voltage V_{bi} of heterojunction of two semiconductors numbered 1 and 2 in thermal equilibrium by the difference of their Fermi levels before contact[5]

$$V_{bi} = \frac{E_{F1} - E_{F2}}{q}, \quad (6)$$

$$E_F(\mathrm{n-type}) = -\chi - \zeta_n, \quad (7)$$

$$E_F(\mathrm{p-type}) = -\chi - E_g + \zeta_p, \quad (8)$$

$$\zeta_n = k_B T \log\left(\frac{N_C}{N_D}\right), \quad (9)$$

$$\zeta_p = k_B T \log\left(\frac{N_V}{N_A}\right), \quad (10)$$

$$V_{bi,n} = V_{bi}\frac{\varepsilon_p N_A}{\varepsilon_p N_A + \varepsilon_n N_D}, \quad (11)$$

$$V_{bi,p} = V_{bi}\frac{\varepsilon_n N_D}{\varepsilon_p N_A + \varepsilon_n N_D}. \quad (12)$$

Built-in voltage is positive is if Fermi level of semiconductor 1 is above the Fermi level of semiconductor 2. For AZO/Cu_2O (Ga_2O_3/Cu_2O) heterojunction, this calculation gives V_{bi} of 0.99 V (1.93 V), respectively.

3 Cu_2O photoelectrode preparation and testing

Electrodeposited copper oxide devices were prepared by the methods described in Dias et al.,[7] with the following specific differences. The sputtered gold layer at the substrate was 150 nm thick. The Cu_2O was deposited for 100 min, yielding polycrystaline films of approximately 500 nm thickness. Atomic layer deposition of AZO was as described in Ref. [7], while ALD of Ga_2O_3 was as described in Pan et al.[21] Each was followed immediately by ALD of 100 nm TiO_2.[7] For the current-voltage data of Figure 2, the devices were first functionalized by RuOx catalyst by electrodeposition, then tested in pH 5 electrolyte, as described in Ref. [7]. For the photovoltage decay experiments, the capacitive nature of RuOx prevented unambiguous measurements of potential. Instead, electrodeposited Pt was used as catalyst, deposited as described in Ref.[23]. Devices of Pt/ TiO_2/Ga_2O_3/Cu_2O and Pt/TiO_2/AZO/Cu_2O showed similar onset potentials as those using RuOx catalyst. In control experiments, the Pt/TiO_2 interface was shown to rapidly and stably equilibrate at 0.0 V vs RHE in the dark when in contact with H2-saturated electrolyte solution. This condition therefore pinned the Pt/TiO_2 surface potential at 0, ideal for open circuit potential measurements without capacitive effects. Hydrogen gas (¿99.99%) was produced by a hydrogen generator and bubbled into the electrolyte at atmospheric pressure. The photocathodes were connected as working electrodes with an Ag/AgCl (3M) reference electrode and a Pt wire counter electrode, held at open circuit using a Bio-Logic SP-200 potentiostat/galvanostat, and illuminated with a "cold white" spectrum LED source (Thorlabs). The light intensity was calibrated to a value which produces the same photocurrent density on the photocathodes as is generated under a class ABB solar simulator (LCS-100, Newport) calibrated at one sun intensity. The open circuit was measured continuously, the device was illuminated for ca. 30 sec to determine the steady-state photopotential, then the LED was switched off by electronic switch to monitor the decay of potential versus time.

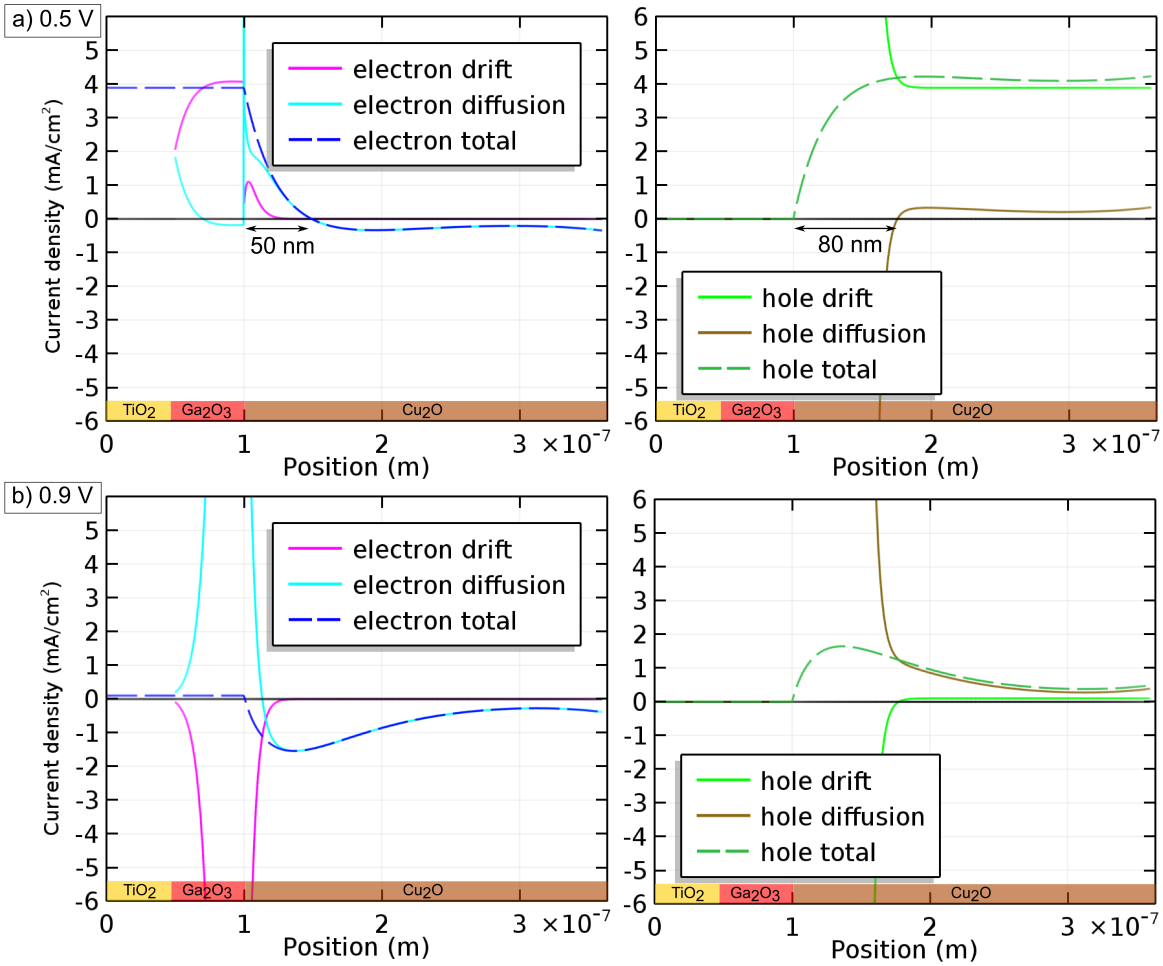

Figure S1: Electron (left column) and hole (right column) current densities and their components for $TiO_2/Ga_2O_3/Cu_2O$ under illumination and a) 0.5 V and b) 0.9 V. For 0.5 V, electrons are carrying the current in TiO_2 and Ga_2O_3, while hole current is zero. In the 50 nm from Ga_2O_3/Cu_2O interface into Cu_2O, electron current flows in the correct direction to the left, while beyond 50 nm the electron current flows in undesired direction to the back contact (negative sign) and hole current compensates this. Looking closer at the diffusion and drift current components, we observe that electron drift current dominates electron current in Ga_2O_3 and electron diffusion current dominates in Cu_2O. Throughout Cu_2O, hole drift interestingly dominates over hole diffusion, although the SCR of Cu_2O does not extend more than 25 nm into Cu_2O. Between Ga_2O_3/Cu_2O interface and 80 nm into Cu_2O, hole diffusion current is actually in wrong direction, but it is compensated by hole drift current. For 0.9 V, the electron and hole currents in Ga_2O_3 and TiO_2 are close to zero, while their non-zero profile in Cu_2O balances out in that region. The electron current is dominated by electron diffusion throughout TiO_2, Ga_2O_3 and Cu_2O. For most of Cu_2O (apart from near interface 1), negative electron current is in the undesired direction, and it is opposed by the positive hole current in the desired direction, thus giving total current 0.1 mA/cm^2. Hole current through Cu_2O is dominated by the hole diffusion component, which is a notable difference to the situation at 0.5 V where hole current was dominated by hole drift. Hole drift current throughout Cu_2O is actually in undesired direction. The range of vertical axis for current density between -6 and +6 mA/cm^2 is chosen to facilitate readability - the peak values are cut off in the plot.

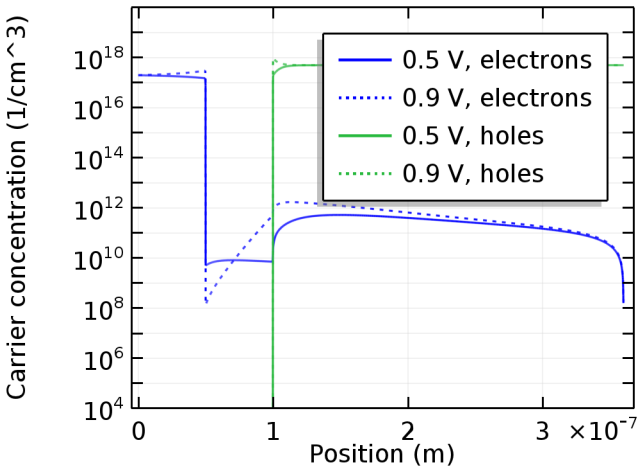

Figure S2: Carrier concentrations for $TiO_2/Ga_2O_3/Cu_2O$ under illumination at 0.5 V (solid lines) and 0.9 V (dashed lines).

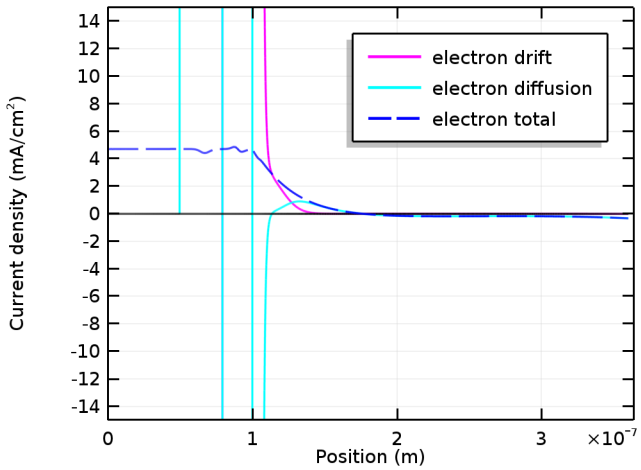

Figure S3: Electron current components for $TiO_2/Ga_2O_3/Cu_2O$ and $N_{D,Ga2O3}$=10^{18} cm^{-3}.

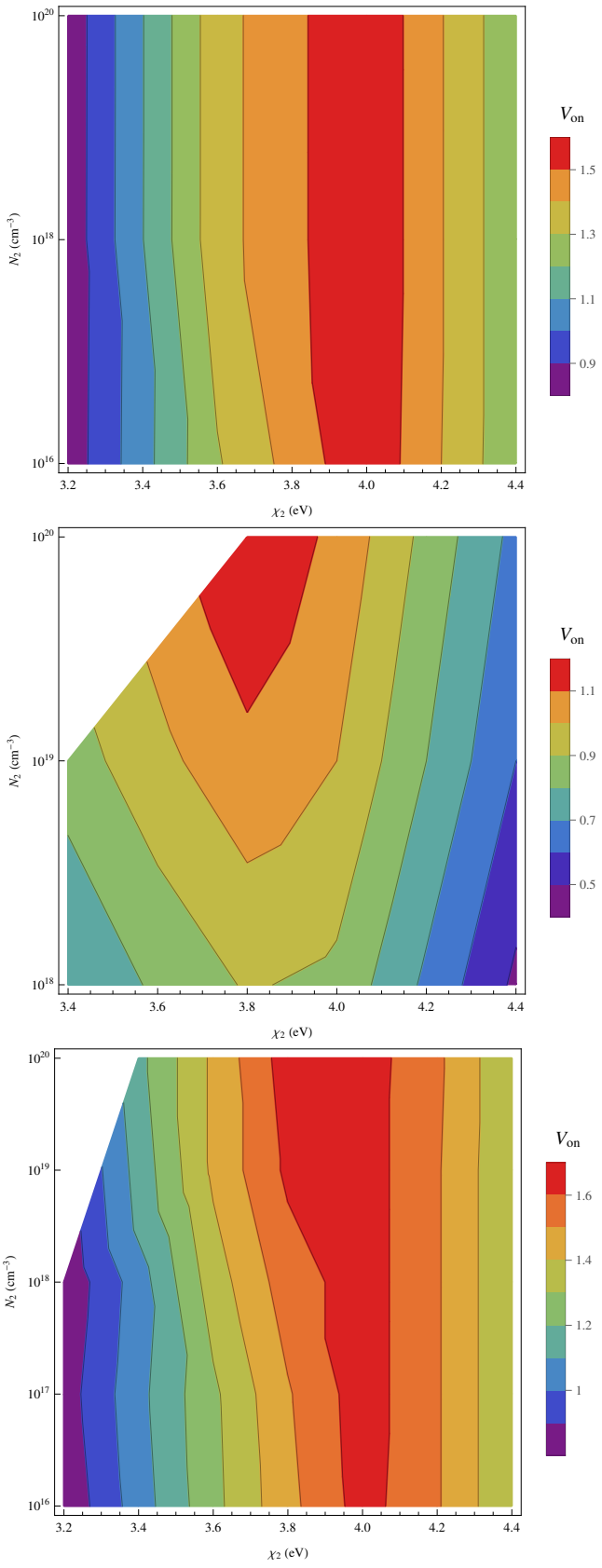

Figure S4: Contour plots of onset voltage for TiO_2/AZO/Cu_2O (top), TiO_2/AZO/IRL/Cu_2O (middle) and TiO_2/Ga_2O_3/Cu_2O (bottom) junctions as function of n-type layer parameters χ_2 and N_2, calculated by SCAPS. The threshold current density 0.5 mA/cm^2 was used for TiO_2/AZO/IRL/Cu_2O junction since the IV curves approach zero more slowly then for TiO_2/Ga_2O_3/Cu_2O junction (where threshold 0.1 mA/cm^2 was used). Simulations were not converging in the blank regions of the contour plot.

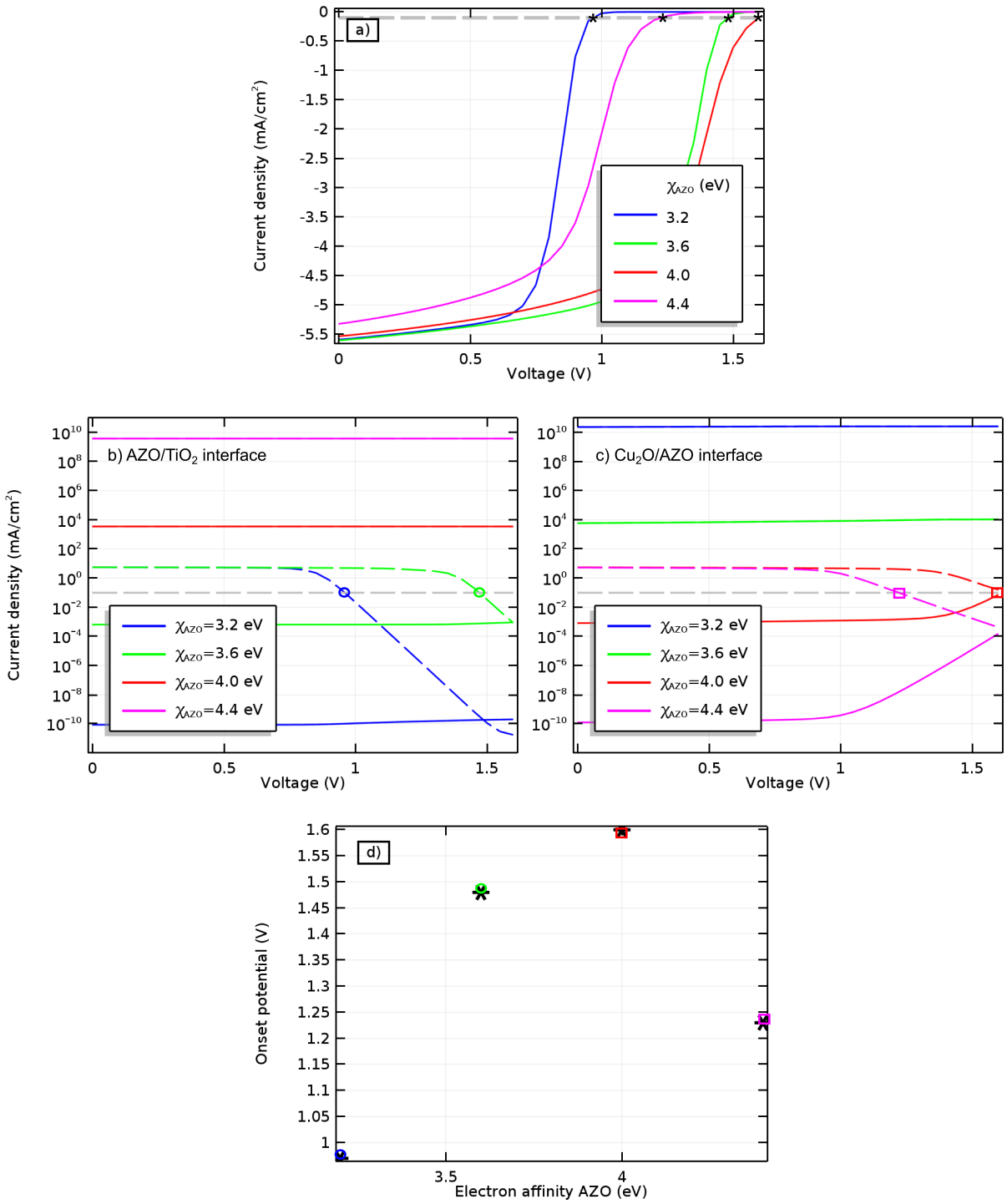

Figure S5: Simulations of transport in TiO_2/AZO/Cu_2O for different values of χ_{AZO} with V_{on} values marked by asterisk. a) Current-voltage curves . Logarithmic plot of electron thermionic current components across b) interface 2 (AZO/TiO_2) j_{nl2} (solid) and j_{nr2} (dashed) and c) interface 1 (Cu_2O/AZO) j_{nl1} (solid) and j_{nr1} (dashed). The intersection of j_{nr} with the threshold current density 0.1 mA/cm^2 is marked by circle for interface 1 and by square for interface 2, with the color corresponding to the respective electron affinity. d) Comparison of extracted values of V_{on} from a) shown as stars and extracted values from analysis in b) and c) shown with the same symbols. Thermionic emission over interface Cu_2O/AZO stops electron current flow for χ_{AZO}=4.0, 4.4 eV , while for χ_{AZO}=3.6 and 3.2 eV the electron thermionic emission over interface from AZO/TiO_2 (interface 2) becomes current limiting.

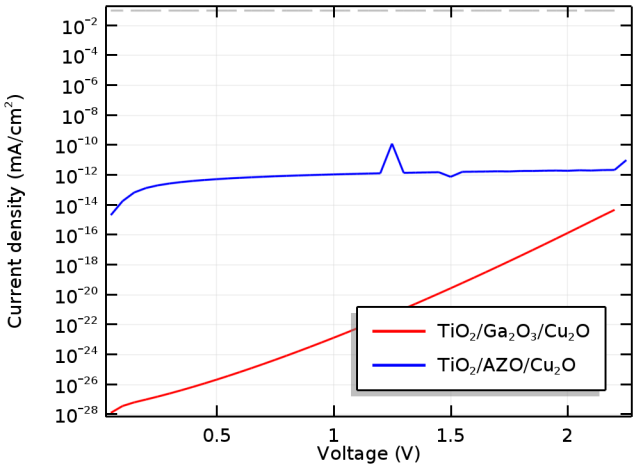

Figure S6: Simulated dark current-voltage curves for $TiO_2/AZO/Cu_2O$ and $TiO_2/Ga_2O_3/Cu_2O$ and forward bias.

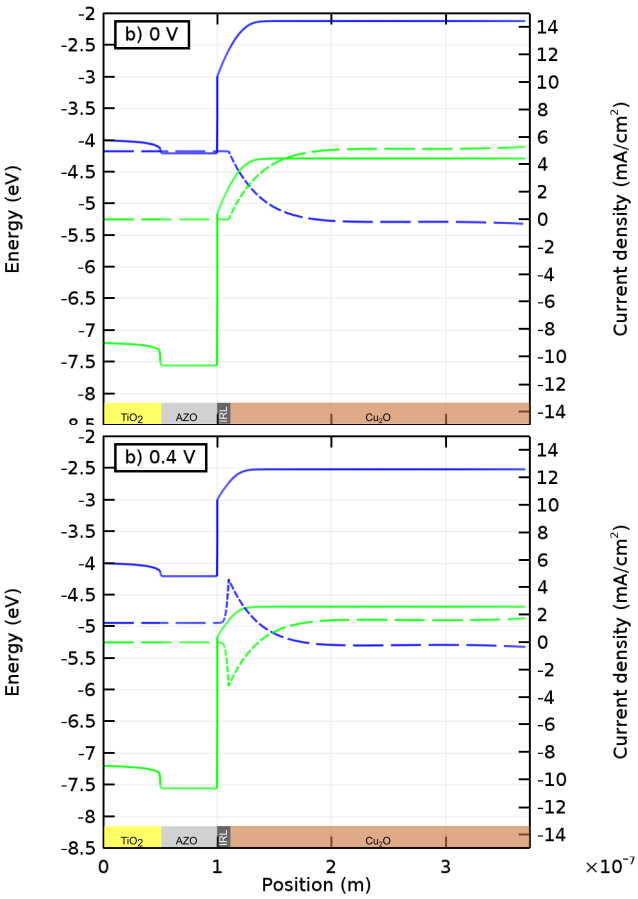

Figure S7: Comparison band diagrams (solid blue/green lines for CB/VB, left axes) and partial current densities (dashed lines, right axes) of $TiO_2/AZO/IRL/Cu_2O$ junction at a) 0 V vs RHE and b) 0.4 V vs RHE.

References

[1] *Comsol Multiphysics 5.3, www.comsol.com.* 2016.

[2] Ya I. Alivov, B. Xiao, S. Akarca-Biyikli, Q. Fan, H. Morkoç, D. Johnstone, O. Lopatiuk-Tirpak, L. Chernyak, and W. Litton. Properties of isotype n-ZnO/n-GaN heterostructures studied by I – V – T and electron beam induced current methods. *Journal of Physics: Condensed Matter*, 20(8):085201, 2008.

[3] Riley E. Brandt, Matthew Young, Helen Hejin Park, Arrelaine Dameron, Danny Chua, Yun Seog Lee, Glenn Teeter, Roy G. Gordon, and Tonio Buonassisi. Band offsets of n-type electron-selective contacts on cuprous oxide (Cu2o) for photovoltaics. *Applied Physics Letters*, 105(26):263901, December 2014.

[4] Zhebo Chen, Todd G. Deutsch, Huyen N. Dinh, Kazunari Domen, Keith Emery, Arnold J. Forman, Nicolas Gaillard, Roxanne Garland, Clemens Heske, Thomas F. Jaramillo, Alan Kleiman-Shwarsctein, Eric Miller, Kazuhiro Takanabe, and John Turner. Flat-Band Potential Techniques. In *Photoelectrochemical Water Splitting*, SpringerBriefs in Energy, pages 63–85. Springer New York, January 2013.

[5] Shun Lien Chuang. *Physics of Optoelectronic Devices*. Wiley, September 1995. Google-Books-ID: ect6QgAACAAJ.

[6] Robert H. Coridan, Adam C. Nielander, Sonja A. Francis, Matthew T. McDowell, Victoria Dix, Shawn M. Chatman, and Nathan S. Lewis. Methods for comparing the performance of energy-conversion systems for use in solar fuels and solar electricity generation. *Energy and Environmental Science*, 8:2886–2901, October 2015.

[7] Paula Dias, Marcel Schreier, S. David Tilley, Jingshan Luo, João Azevedo, Luísa Andrade, Dongqin Bi, Anders Hagfeldt, Adélio Mendes, Michael Grätzel, and Matthew T. Mayer. Transparent Cuprous Oxide Photocathode Enabling a Stacked Tandem Cell for Unbiased Water Splitting. *Advanced Energy Materials*, 5(24):1501537, December 2015.

[8] Brendan Enright and Donald Fitzmaurice. Spectroscopic Determination of Electron and Hole Effective Masses in a Nanocrystalline Semiconductor Film. *The Journal of Physical Chemistry*, 100(3):1027–1035, January 1996.

[9] Markus Gloeckler, James R. Sites, and Wyatt K. Metzger. Grain-boundary recombination in Cu(In,Ga)Se2 solar cells. *Journal of Applied Physics*, 98(11):113704, December 2005.

[10] Haiying He, Roberto Orlando, Miguel A. Blanco, Ravindra Pandey, Emilie Amzallag, Isabelle Baraille, and Michel Rérat. First-principles study of the structural, electronic, and optical properties of ${\textbackslashmathrm{Ga}}_{2}{\textbackslashmathrm{O}}_{3}$ in its monoclinic and hexagonal phases. *Physical Review B*, 74(19):195123, November 2006.

[11] M. D. Heinemann, J. Berry, G. Teeter, T. Unold, and D. Ginley. Oxygen deficiency and Sn doping of amorphous Ga2o3. *Applied Physics Letters*, 108(2):022107, January 2016.

[12] Shogo Ishizuka, Shinya Kato, Takahiro Maruyama, and Katsuhiro Akimoto. Nitrogen Doping into Cu $_2$ O Thin Films Deposited by Reactive Radio-Frequency Magnetron Sputtering. *Japanese Journal of Applied Physics*, 40(Part 1, No. 4B):2765–2768, April 2001.

[13] Jonathan Lee, Elena Flitsiyan, Leonid Chernyak, Jiancheng Yang, Fan Ren, Stephen J. Pearton, Boris Meyler, and Y. Joseph Salzman. Effect of 1.5 MeV electron irradiation on β-Ga2o3 carrier lifetime and diffusion length. *Applied Physics Letters*, 112(8):082104, February 2018.

[14] M. R. Lorenz, J. F. Woods, and R. J. Gambino. Some electrical properties of the semiconductor β?Ga2o3. *Journal of Physics and Chemistry of Solids*, 28(3):403–404, March 1967.

[15] Claudia Malerba, Francesco Biccari, Cristy Leonor Azanza Ricardo, Mirco D'Incau, Paolo Scardi, and Alberto Mittiga. Absorption coefficient of bulk and thin film Cu2o. *Solar Energy Materials and Solar Cells*, 95(10):2848–2854, October 2011.

[16] H. Paul Maruska and Amal K. Ghosh. Transition-metal dopants for extending the response of titanate photoelectrolysis anodes. *Solar Energy Materials*, 1(3):237–247, March 1979.

[17] Takashi Minemoto and Jasmeen Julayhi. Buffer-less Cu(In,Ga)Se2 solar cells by band offset control using novel transparent electrode. *Current Applied Physics*, 13(1):103–106, January 2013.

[18] Takashi Minemoto and Masashi Murata. Theoretical analysis on effect of band offsets in perovskite solar cells. *Solar Energy Materials and Solar Cells*, 133:8–14, February 2015.

[19] Kotaro Mizuno, Masanobu Izaki, Kuniaki Murase, Tsutomu Shinagawa, Masaya Chigane, Minoru Inaba, Akimasa Tasaka, and Yasuhiro Awakura. Structural and Electrical Characterizations of Electrodeposited p-Type Semiconductor Cu2o Films. *Journal of The Electrochemical Society*, 152(4):C179–C182, April 2005.

[20] NREL. *Solar Spectral Irradiance: Air Mass 1.5 (accessed March 17, 2012), http://rredc.nrel.gov/solar/spectra/am1.5/.*

[21] Linfeng Pan, Jin Hyun Kim, Matthew T. Mayer, Min-Kyu Son, Amita Ummadisingu, Jae Sung Lee, Anders Hagfeldt, Jingshan Luo, and Michael Grätzel. Boosting the performance of Cu 2 O photocathodes for unassisted solar water splitting devices. *Nature Catalysis*, 1:412–420, May 2018.

[22] Adriana Paracchino, Jan Cornelius Brauer, Jacques-Edouard Moser, Elijah Thimsen, and Michael Graetzel. Synthesis and Characterization of High-Photoactivity Electrodeposited $Cu_2$$O Solar Absorber by Photoelectrochemistry and Ultrafast Spectroscopy. *The Journal of Physical Chemistry C*, 116(13):7341–7350, April 2012.

[23] Adriana Paracchino, Vincent Laporte, Kevin Sivula, Michael Graetzel, and Elijah Thimsen. Highly active oxide photocathode for photoelectrochemical water reduction. *Nat Mater*, 10(6):456–461, June 2011.

[24] Sebastian Siol, Jan C. Hellmann, S. David Tilley, Michael Graetzel, Jan Morasch, Jonas Deuermeier, Wolfram Jaegermann, and Andreas Klein. Band Alignment Engineering at Cu2o/ZnO Heterointerfaces. *ACS Applied Materials & Interfaces*, 8(33):21824–21831, August 2016.

[25] Yuki Takiguchi and Shinsuke Miyajima. Device simulation of cuprous oxide heterojunction solar cells. *Japanese Journal of Applied Physics*, 54(11):112303, November 2015.